Brain and Spine 4 (2024) 102772

Contents lists available at ScienceDirect

Brain and Spine

journal homepage: www.journals.elsevier.com/brain-and-spine

Mathematical modelling of cerebral haemodynamics and their effects on ICP

Ka Hing Chu [a,*], Ihsane Olakorede [a], Erta Beqiri [a], Marek Czosnyka [a], Peter Smielewski [a]

[a] Brain Physics Laboratory, Division of Neurosurgery, Department of Clinical Neurosciences, University of Cambridge, UK

ARTICLE INFO

Handling Editor: Dr W Peul

Keywords:
Mathematical modelling
Intracranial pressure
Cerebral hemodynamics
Interstitial fluid

ABSTRACT

Introduction: Electrical-equivalence mathematical models that integrate vascular and cerebrospinal fluid (CSF) compartments perform well in simulations of dynamic cerebrovascular variations and their transient effects on intracranial pressure (ICP). However, ICP changes due to sustained vascular diameter changes have not been comprehensively examined. We hypothesise that changes in cerebrovascular resistance (CVR) alter the resistance of the bulk flow of interstitial fluid (ISF).

Research question: We hypothesise that changes in CVR alter the resistance of the bulk flow of ISF, thus allowing simulations of ICP in response to sustained vascular diameter changes.

Material and methods: A lumped parameter model with vascular and CSF compartments was constructed and converted into an electrical analogue. The flow and pressure responses to transient hyperaemic response test (THRT) and CSF infusion test (IT) were observed. Arterial blood pressure (ABP) was manipulated to simulate ICP plateau waves. The experiments were repeated with a modified model that included the ISF compartment.

Results: Simulations of the THRT produced identical cerebral blood flow (CBF) responses. ICP generated by the new model reacted in a similar manner as the original model during ITs. Plateau pressure reached during ITs was however higher in the ISF model. Only the latter was successful in simulating the onset of ICP plateau waves in response to selective blood pressure manipulations.

Discussion and conclusion: Our simulations highlighted the importance of including the ISF compartment, which provides mechanism explaining sustained haemodynamic influences on ICP. Consideration of such interactions enables accurate simulations of the cerebrovascular effects on ICP.

1. Introduction

Intracranial pressure (ICP) is a vital quantity to be monitored for clinical decisions in neurointensive care, and substantial effort has been made to investigate its dynamics with mathematical modelling. Works by Monro and Kellie (Kellie, 1824; Monro, 1783) described the volume conservation of fluids and brain matter within the skull due to the unique intracranial structure: the systems of cerebral blood flow (CBF) and cerebrospinal fluid (CSF) circulation are embedded in the brain tissue, which in turn is constrained by the rigid dura and cranium. This indicates that the changes in fluid flow at different time scales contribute to ICP variations in different ways. Subsequent studies have explored the transient and sustained effects of CSF flow on ICP. Notably, Davson (Davson et al., 1970) attributed the steady-state changes in ICP to the formation rate of CSF, the resistance of CSF outflow through the skull, and the pressure at the sagittal sinus where CSF absorption occurs. On the other hand, Marmarou (Marmarou et al., 1975; Marmarou et al., 1978) introduced the concept of intracranial compliance in his modelling studies, and demonstrated its role on the dynamic aspects of ICP.

The interactions between cerebral haemodynamics and ICP is of much interest, particularly in scenarios like traumatic brain injury. Importantly, Ursino (Ursino, 1988a, 1988b; Ursino and Lodi, 1997; Ursino and Di Giammarco, 1991) included in his model a representation of cerebrovascular circulation; this enabled the simulations of physiological phenomena involving vascular dilation and constriction such as cerebral autoregulation. However, it is common for modelling studies to integrate compartments of CBF and CSF circulation to explore their combined effects on ICP. While these models are highly successful in illustrating the dynamic effects of fluid flow, they may be less robust in representing long-term interactions between cerebral blood volume (CBV) and ICP. Simulations with such models could therefore be inaccurate when attempting to reflect clinical phenomena caused by prolonged changes in CBV, such as sustained vasodilation.

* Corresponding author. Brain Physics Laboratory, Division of Neurosurgery, Dept of Clinical Neurosciences, University of Cambridge, UK.
E-mail address: khc42@cam.ac.uk (K.H. Chu).

https://doi.org/10.1016/j.bas.2024.102772
Received 2 July 2023; Received in revised form 17 January 2024; Accepted 18 February 2024
Available online 19 February 2024
2772-5294/© 2024 The Authors. Published by Elsevier B.V. on behalf of EUROSPINE, the Spine Society of Europe, EANS, the European Association of Neurosurgical Societies. This is an open access article under the CC BY-NC-ND license (http://creativecommons.org/licenses/by-nc-nd/4.0/).

Abbreviations

ABP –	arterial blood pressure
ICP –	intracranial pressure
CPP –	cerebral perfusion pressure
TBI –	traumatic brain injury
ISF –	interstitial fluid
CSF –	cerebrospinal fluid
CVR –	cerebrovascular resistance
CBF –	cerebral blood flow
CBV –	cerebral blood volume
THRT –	transient hyperaemic response test
IT –	infusion test

In an attempt to represent the intracranial pressure-volume relationships of patients with cerebral oedema, Doron et al. (2021) incorporated into their electrical model volume changes of brain tissue. In addition to elements representing the subarachnoid space, ventricles and cerebral vasculature, a new compartment was added into the model, depicting the bulk flow of cerebral interstitial fluid (ISF). This compartment was characterised by a resistive element to represent the resistance of ISF circulation through the brain parenchyma into the subarachnoid space. This novel design was based on the theory that cellular swelling reduces the volume of cerebral extracellular space, hence narrowing the channels through which cerebral ISF can flow (HANSEN and OLSEN, 1980; Ramirez de Noriega et al., 2018). With a set of differential equations relating the pressure to volume at each compartment, the model allowed the changes in brain volume to interact with ICP dynamics. Simulations with this approach successfully mimicked various physiological features, in particular the elevated ICP and reduced ventricular volume observed in patients with cerebral oedema and disruption of the blood-brain barrier.

Doron's work provided a modelling mechanism for sustained interactions among the resistances of fluid flow, compartmental volumes and ICP, via the ISF circulation compartment. This is especially important when investigating phenomena involving the interplay between CBV and ICP. A notable example is cerebral autoregulation, a homeostatic mechanism of the vascular system to stabilise the cerebral blood flow (CBF), in spite of variations in cerebral perfusion pressure. Resistive cerebral arterioles react to changes in perfusion pressure or vasoactive stimuli such as carbon dioxide (Brady et al., 2012; Claassen et al., 2021) by actively controlling the myogenic tone of the vessel walls, in order to dilate or constrict. This alters the cerebrovascular resistance (CVR) of the vessels and hence the CBV. Intracranial pathologies such as traumatic brain injuries often cause reduction in intracranial compliance,

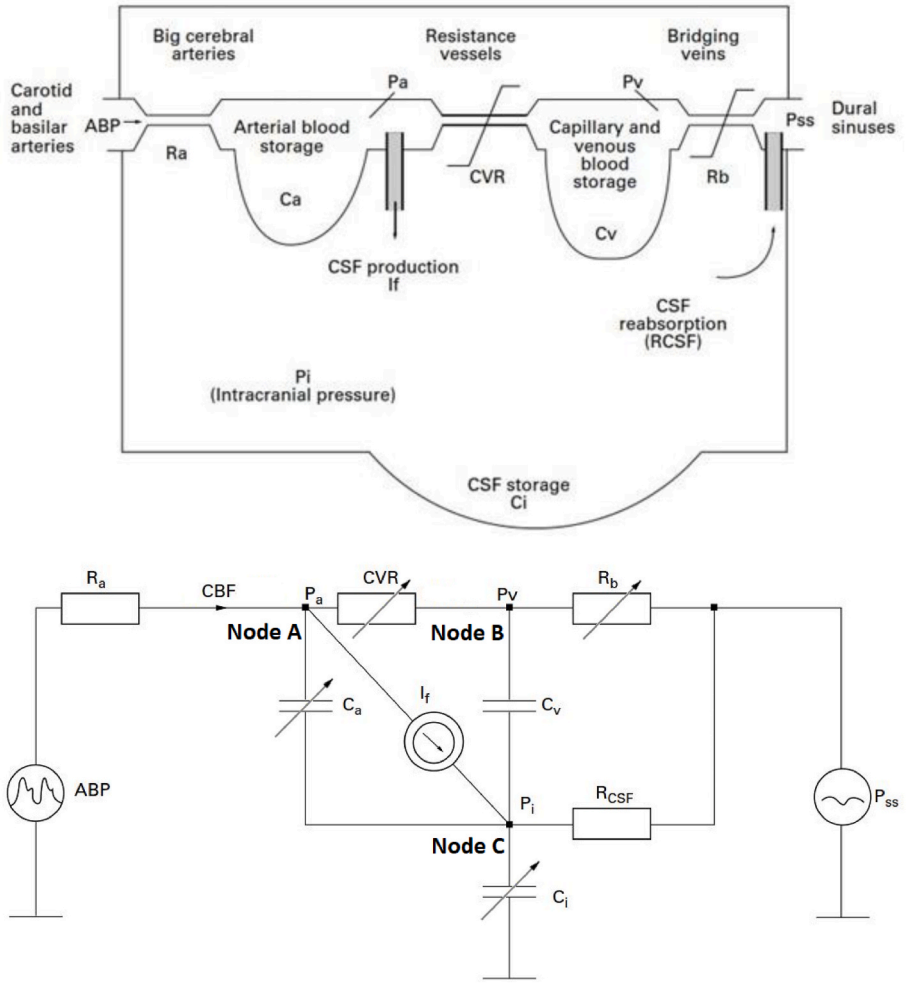

(b)

Fig. 1. (Czosnyka et al., 1997). The unilateral hydrodynamic model proposed by Czosnyka (a) and its electrical analogue (b). State equations are derived by considering the flow of current in nodes A, B and C (located in the arterial, venous and CSF compartments respectively).

rendering the intracranial compartment susceptible to CBV increase, and resulting in ICP surges, falls in cerebral perfusion pressure (CPP) and consequently in secondary brain insults (Liu et al., 2020). It is therefore crucial for models of intracranial hydrodynamics to capture the effects of cerebral haemodynamics on ICP. In this study, we built on a classical model of CBF and CSF circulation, and incorporated a compartment depicting the flow of cerebral ISF. With this model we attempted to replicate various pathophysiological features observed in clinical data.

2. Material and Methods

2.1. Construction of the electric analogue model

This study initially replicated the unilateral hydrodynamic model proposed by Czosnyka (Czosnyka et al., 1997) (Fig. 1(a)). The electrical analogue of the model (Fig. 1(b)) consists of four resistive (R_a, CVR, R_b, and R_{CSF}) and three capacitive (C_a, C_v, and C_i) components, the meaning of which will be described in detail below. It also includes two input voltage sources ABP and P_{ss}, representing the systemic arterial blood pressure and the venous pressure in the dural sinuses respectively.

A mathematical description of the resistive and capacitive elements in the model is provided in the Appendix section.

2.2. Modifications to the model

To provide a mechanism for pressure interactions between the cerebrovascular and intracranial compartments, a representation of ISF circulation was added to the model. In the electrical analogue, it was depicted as a pathway with a resistive component (Fig. 2).

It is postulated that vasodilation (represented as reduction in CVR and increased volume in the arterial bed) would cause reduction in ISF space volume (depicted as increased R_{ISF}). As there is currently a lack of experimental data quantifying this interaction, we have simply modelled R_{ISF} as being reciprocally related to the CVR as the first approximation.

$$R_{ISF} = \frac{R_{ISFspan}}{CVR} + R_{ISFoffset}$$

where $R_{ISFspan}$ and $R_{ISFoffset}$ are constants.

2.3. Experiments

A programme designed to be run on Windows 10 was written in Object Pascal (Embarcadero Delphi 10.2) using the RAD studio. After selecting either the original or the new model and importing ABP data from a csv file, the programme used a set of equations (described in the Appendix section) to evaluate and plot P_a, P_v, P_i, and CBF against time.

Three pathophysiological phenomena observed in clinical data were simulated by the programme to test and compare the performances of the models:

1. Transient hyperaemic response test (THRT) – a diagnostic test assessing the capacity of cerebral autoregulation. During the test, the common carotid artery was compressed for a few seconds before being released, with a transient increase in cerebral blood flow indicating intact cerebral autoregulation mechanism (Mahajan and Simpson, 1998; Smielewski et al., 1995).
2. CSF infusion test – a clinical study used to analyse the dynamics of CSF circulation in patients suspected of normal pressure hydrocephalus. In a lumbar infusion study, artificial CSF is infused at a constant rate into the CSF space via a lumbar puncture, causing the ICP to rise to a plateau level (determined by a balance of extra fluid infusion and increased pressure-gradient driven CSF outflow) (Ekstedt, 1977; Lalou et al., 2020; Czosnyka et al., 2004; Davson et al., 1970; Caire and Moreau, 2010; Oertel and Antes, 2013).
3. ICP plateau waves – a sudden surge in ICP to a plateau with a duration of 5–20 min, commonly seen in TBI patients with intact autoregulatory capabilities (Czosnyka et al., 1999; Daley et al., 2005; Lundberg, 1962). It has been suggested (Rosner et al., 1995) that plateau waves are caused by a vasodilatory cascade (Fig. 3), where the resistive arterioles dilate due to autoregulation in response to an initial, abrupt, drop in ABP. The effect of increasing cerebral blood volume (CBV) is then transmitted to the intracranial compartment and raises the ICP, causing further reduction in CPP. This vicious cycle results in the continuous rise in ICP until the vessels have

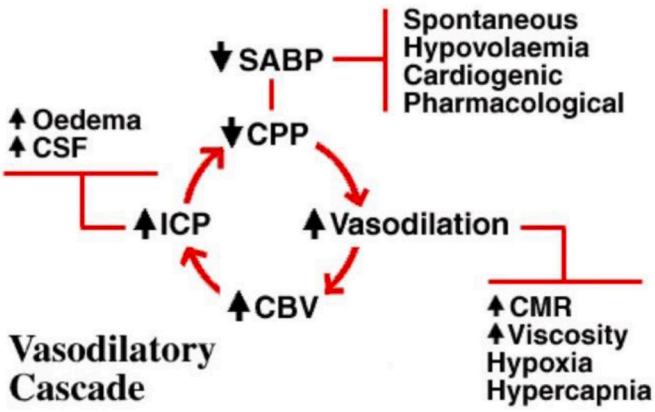

Fig. 3. (Rosner et al., 1995). Illustration of factors contributing to vasodilatory cascades.

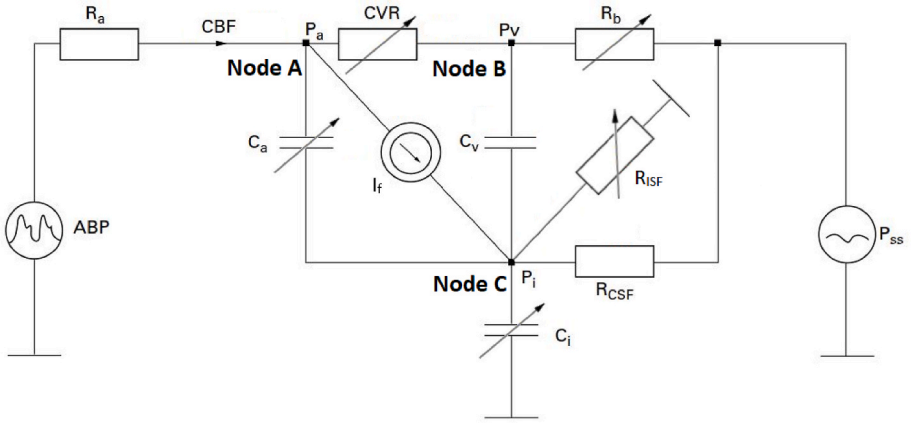

Fig. 2. The modified unilateral model with added ISF compartment, represented by a resistive component (R_{ISF}).

exhausted their capacity to dilate, and occurs despite blood pressure restoration which may follow the transient drop.

Examples of clinical recordings depicting the pathophysiological phenomena mentioned above were included in Fig. 4:

3. Results

3.1. Transient hyperaemic response test

The compression of the common carotid artery was represented by a step drop in ABP, before being restored to its original level (Fig. 5 (a)). The responses of CBF and CVR are shown in Fig. 5 (b) and (c) respectively.

The CBF simulated by the original was reduced during the compression, provoking visible compensatory vasodilation (decrease in CVR during the compression). After the compression was released, CBF surged before falling gradually to the level before the compression (as CVR returned to its baseline value due to active vasoconstriction). CBF generated by the new model reacted to the step changes in ABP identically: it was suppressed during the compression, before overshooting and returning to the baseline level as the compression was released. This shows that the simulations with both models were able to produce the transient hyperaemic response observed in transcranial Doppler (TCD) ultrasonography recordings (Mahajan and Simpson, 1998).

3.2. Infusion test

For the simulations of an infusion stage between t_{start} and t_{stop}, a constant term I_{inf} was added to the rate of CSF formation (I_f) to represent

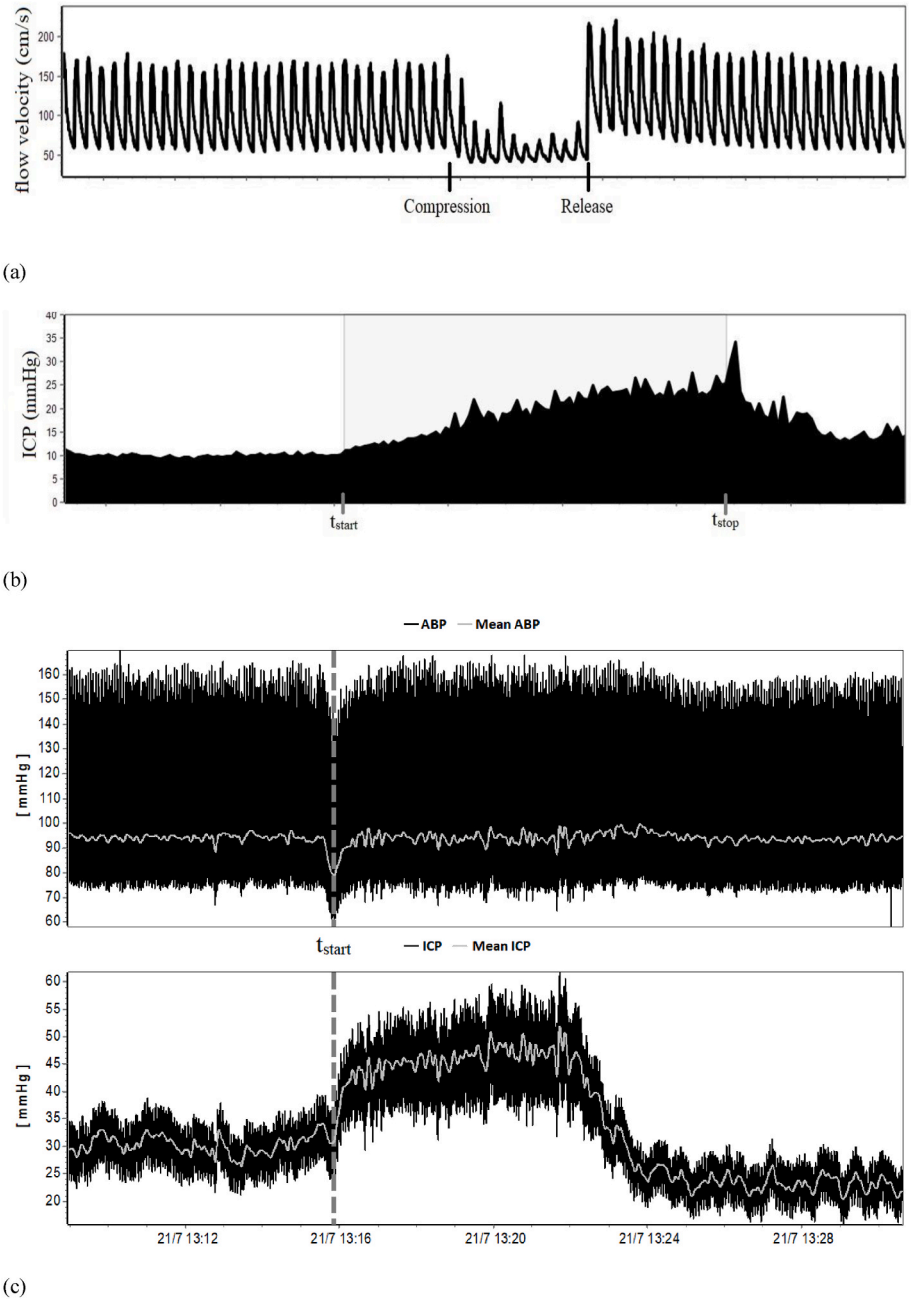

Fig. 4. Clinical recordings of the three pathophysiological phenomena to be simulated by the model: (a) transient hyperaemic response test (THRT), (b) CSF infusion test, and (c) ICP plateau waves (where a rapid rise in ICP was triggered by a sudden drop in ABP, beginning from t_{start}).

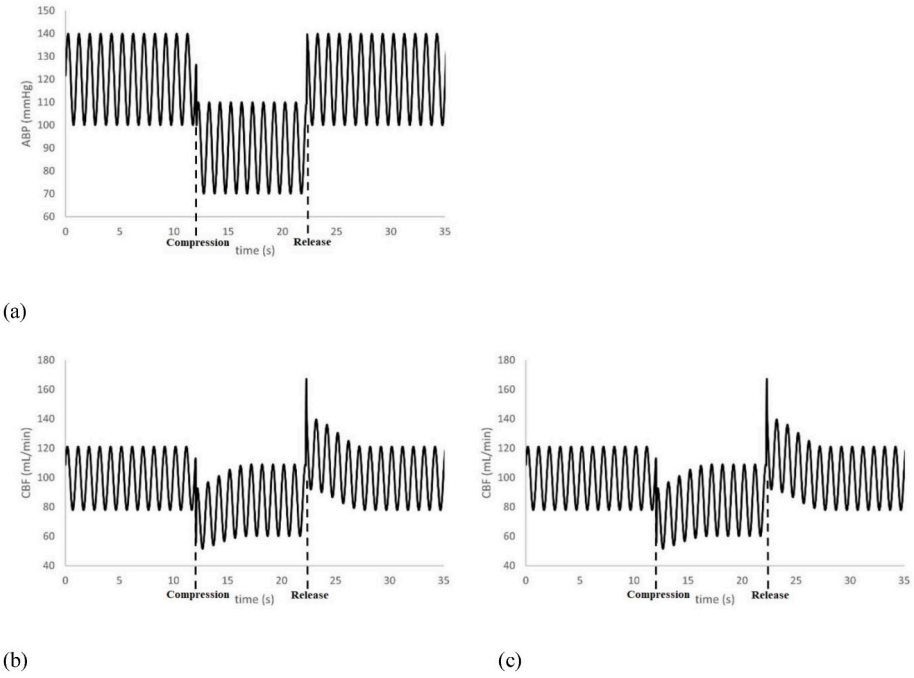

Fig. 5. Simulations of THRT with step changes in ABP between the onset and release of artery compression (a), and the CBF responses with the new (b) and original (c) models.

the rate of infusion into the CSF space. The ICP responses are plotted in Fig. 6 (a), while Fig. 6 (b) and (c) illustrate the intracranial pressure-volume relationships of the models, evaluated with the ICM+® software.

Simulations with both models produced the ICP behaviour commonly seen in real clinical recordings, rising to a plateau during the infusion stage and falling back to the baseline level when the infusion was terminated. However it is worth noting that the ICP generated by the new model rose to a higher level before levelling off; this resulted in a slightly higher value of R_{CSF} produced by the new model.

3.3. Plateau wave

ICP plateau waves were simulated by creating step changes in ABP (Fig. 7 (a)). It was reduced by 10 mmHg initially (stage A), before being raised back to its baseline value (stage B). It was then further increased by 10 mmHg (stage C), and again restored to the baseline level (stage D). In order to produce a significant rise in ICP, the elasticity parameter (E) was set as 0.25, as opposed to 0.05 as in the two previous experiments.

The models produced very different results. In the new model, a drop in ABP triggered a rise in ICP from its baseline value (18 mmHg) to a plateau level of 43 mmHg within 5 min. Raising the ABP back to its initial value caused the ICP to increase momentarily, before stabilising at a slightly lower level (41 mmHg). Further increase in ABP resulted in a rapid drop of ICP until it flattened slightly below the baseline value (16 mmHg). A final restoration of ABP to its initial level brought the ICP back to its baseline. On the other hand, ICP simulated by the original model displayed momentary perturbations in response to each step change in ABP. However, it always returned to its baseline level of 18 mmHg; it was not able to simulate the onset of a plateau wave.

4. Discussion

The pressure-flow interactions of each compartment enabled the original model to simulate various physiological responses of flow and pressure commonly observed in clinical practice. For instance, the haemodynamic representation has been successful in simulating the behaviours of CBF in response to changes in CPP; this has allowed the demonstration of the effects of cerebral autoregulation: simulations of THRT have created the characteristic transient hyperaemic responses, which is caused by the vasodilation of resistive arterioles in response to the step drop in ABP. Moreover, the intracranial compartment correctly simulated the response of ICP to constant rate infusion.

However, the sustained effects of vascular constriction and dilation on ICP (such as plateau waves) could not be reflected correctly by the model: in a model consisting of only the vascular and CSF compartments, the state equation in a steady state (without current passing through the dynamic pathways) at node C is reduced as

$$I_f = \frac{P_i - P_{ss}}{R_{csf}}$$

which is the Davson's equation. As I_f, R_{CSF} and P_{ss} are all modelled as constants, P_i (ICP) must also be a constant. This explains why the simulated ICP always returns to a constant value after responding initially to a change in ABP. As a result, the original model cannot transmit any long-term volume changes in the vasculature to the intracranial compartment. Without modifications to the model, any clinical phenomena involving prolonged interactions between the two cannot be simulated correctly. To rectify this, a new static mechanism must be added to link the fluid dynamics in the arterial and intracranial compartments.

Recent studies have established the physiological bases of cerebral ISF circulation (Syková and Nicholson, 2008; Abbott, 2004) and examined its impairment in intracranial pathologies (Hrabětová et al., 2003; Iliff et al., 2014). These findings allowed the mathematical representation of intracellular swelling as the rise in ISF flow resistance, and the reduction in extracellular space volume (HANSEN and OLSEN, 1980; Ramirez de Noriega et al., 2018). With the incorporation of this mechanism, the modelling work by Doron et al. (2021) accurately reproduced the elevated ICP due to brain swelling. This study postulated that the dilation of resistive cerebral arterioles can cause the narrowing of the ISF circulation channels, in a similar manner as in cerebral oedema. With the addition of this static pathway, simulated vascular constrictions and dilations can cause persistent changes in ICP. As there is currently a lack of quantitative evidence supporting this hypothesis, the

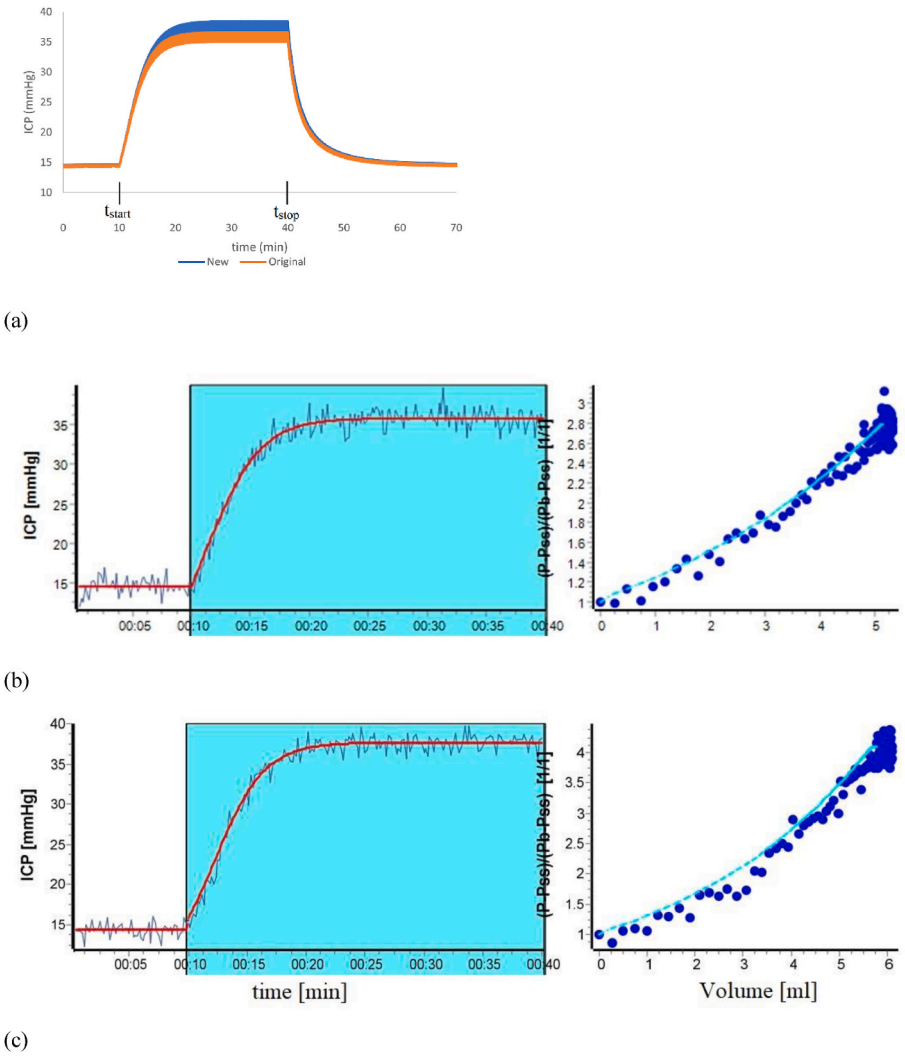

Fig. 6. Simulations of the infusion tests (between t_{start} and t_{stop}) with the models (a); and the analysis with the ICM+® software, illustrating the pressure-volume relationships represented by the original (b) and new (c) models; the R_{CSF} were evaluated to be 13.86 and 14.72 mmHg/mL/min respectively. For illustrative purposes in the curve-fitting process, white noises were added to the generated ICP.

CVR and R_{ISF} were assumed to follow a reciprocal relationship; this serves as a simplification to the intracranial pressure-volume interaction in reality. Due to the current incomplete understanding of the dynamics of the ISF pathway, it was assumed in the first approximation that the ISF sink pressure is constant. From the perspective of modelling, given we are at this point not interested in estimating the ISF flow itself, it makes no difference if the pressure in this topology is set as zero or other constant values.

Our modified model has proved to be successful in simulations of responses to various physiological simulations. Notably, with increasing ABP (Fig. 7), the ICP responses produced by the models were markedly different, with the new model accurately reflecting the reduction in ICP with increasing CPP within the range of autoregulation. This is because its inclusion of the ISF compartment allowed the effects of changing CBV in the arterial compartment to be transmitted to the ICP in the intracranial compartment, which the original model failed to represent. When generating plateau waves (Fig. 7), this transmission is responsible for completing the cycle of vasodilatory cascade, resulting in the rapid rise in ICP as observed in clinical data.

Previous work by Ursino and Giammarco (Ursino and Di Giammarco, 1991) also attempted to generate the plateau waves. Compared to their study, our approach aims to describe the phenomena of cerebrovascular dynamics with a model that is as simple as possible, which only requires a minimal number of parameters. Our ultimate goal is to estimate these parameters from multimodal neuro-monitoring time series data. Examples of such estimations using our model can be found in the works studying C_a, C_i, CVR and critical closing pressure based on Transcranial Doppler Ultrasonography (Czosnyka et al., 1997; Varsos et al., 2014), and R_{CSF} and C_i using infusion tests (Czosnyka et al., 2008). Thus, the model has proven itself as a practical base for interpretation of the neuro-monitoring data. With a slight modification to the model, it became possible to demonstrate the intracranial pressure-volume interactions through the generation of plateau waves, and thereby improving the reliability of parameter estimations.

A thorough understanding of the interactions between the haemodynamics and ICP is also important to the interpretation of clinical data related to disturbed CSF circulation. A notable example is the treatment of patients with hydrocephalus; their symptoms can be alleviated with the surgical insertion of a shunt, which drains CSF from the brain to the abdominal cavity. A good prognostication of improvement after shunting requires the accurate estimation of key parameters describing the CSF dynamics, one of which is the resistance of CSF outflow (R_{CSF}). This can be achieved through the simulation of a post-shunting infusion test. The evaluation of R_{CSF} is conventionally based on a model of CSF circulation (Eklund et al., 2007); it is calculated with the following formula:

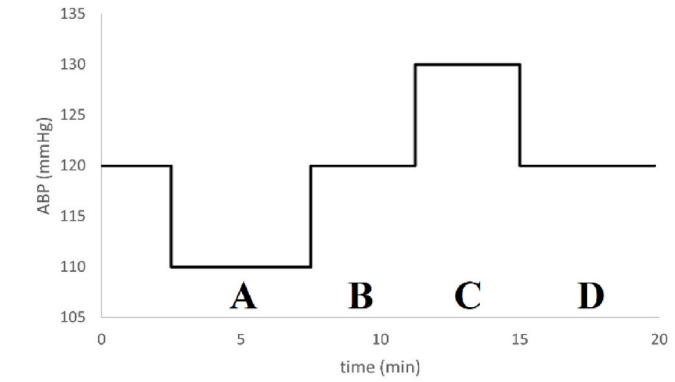

(a)

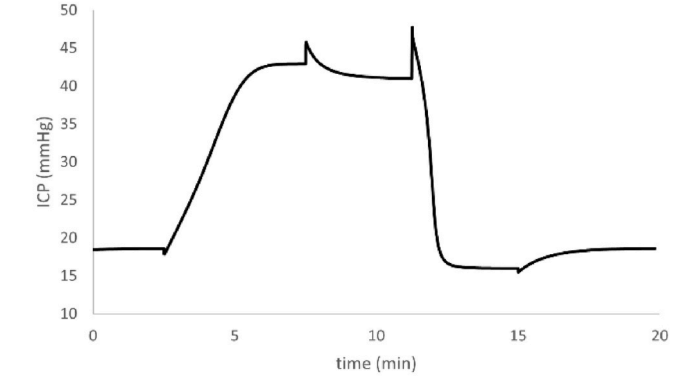

(b)

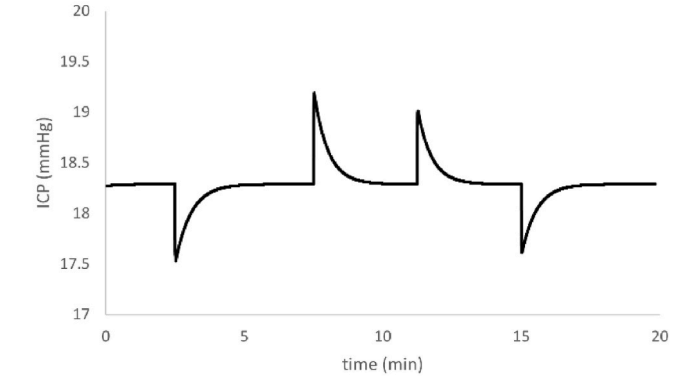

(c)

Fig. 7. Simulated ICP for the new (b) and original (c) models, in response to step changes in ABP (a).

$$R_{CSF} = \frac{P_{plateau} - P_{baseline}}{I_{inf}}$$

Where $P_{baseline}$ and $P_{plateau}$ are the ICP at baseline and plateau levels respectively at the infusion test.

Simulations with the new model in this study (Fig. 6) showed that the rise in ICP resulted in vasodilation, which in turn raised the ICP to a higher level than the original model. This suggests that apart from R_{CSF}, the autoregulation capacity can be another factor determining the ICP dynamics in an infusion study. A mathematical model considering only the CSF compartment may neglect the influence of CBV on ICP, and mistakenly attributing it to R_{CSF}. Theoretically this can result in the overestimation of R_{CSF}. Previous studies have shown that the positive predictive power of R_{CSF} has been clinically acceptable (Eklund et al., 2007), with recommended the R_{CSF} threshold for shunting to be between 13 and 18 mmHg/ml/min (Boon et al., 1997; Børgesen and Gjerris, 1982). The extra increase in ICP is likely to be small in patients diagnosed for normal pressure hydrocephalus, and thus a small overestimation of R_{CSF} may be on limited clinical significance. Nevertheless, this effect is worth exploring further with concurrent measurements of the strength of cerebral autoregulation during infusion tests.

5. Conclusions

This study investigated the relationships between cerebral blood volume and ICP with an intracranial hydrodynamic model, which was modified to include a compartment representing the circulation of cerebral ISF and coupled with the cerebrovascular compartment. The modified model was successful in depicting features of intracranial physiology involving the prolonged interplay between CBV and ICP.

Funding

Erta Beqiri is supported by the Medical Research Council (grant no.: MR N013433-1) and by the Gates Cambridge Scholarship.

Declaration of competing interest

The authors declare the following financial interests/personal relationships which may be considered as potential competing interests:

Peter Smielewski, Marek Czosnyka has patent with royalties paid to Cambridge Enterprise Ltd, University of Cambridge, Cambridge.

Appendix

Mathematical description of the model

This section presents a detailed description of the parameters used in the model.

R_a

Although the resistance at the large cerebral arteries can be increased permanently in pathological conditions such as atherosclerosis and vasospasm (Czosnyka et al., 1997), its dynamic responses to changes in cerebral perfusion pressure is negligible when compared to the smaller resistive arterioles, and is therefore modelled as a constant.

CVR

The effect of cerebral autoregulation is considered when modelling the cerebrovascular resistance of the arterioles: to simulate the dilation and constriction of the resistive vessels in response to cerebral perfusion pressure, the model uses the inverse of a 6th order polynomial to relate CPP to CVR (Hoffmann, 1987).

$$CVR(CPP_m) = CVR_{max} - \frac{CVR_{max} - CVR_{min}}{1 + \left(\frac{CPP_m + CPP_{offset}}{CPP_{max} - CPP_{min}}\right)^6}$$

where.

CVR_{max} and CVR_{min} are the CVR during maximal vasoconstriction and vasodilation,

CPP_{max} and CPP_{min} are the upper and lower limits of autoregulation,

CPP_{offset} is a constant translating the CVR-CPP curve, and.

CPP_m is the mean cerebral perfusion pressure, averaging the CPP values in the last 6 s to simulate the high pass filter, time lagged, character of the delayed autoregulatory response (Aaslid et al., 1989).

Ca

The compliance of the cerebrovascular bed can be described as a non-linear function of either CVR (Piechnik, 2000) or CPP (Drzewiecki et al., 1997). The 'CVR reciprocal' option was chosen for this model, so that the compliance depends on the delayed response of the vascular muscle:

$$C_a = \frac{C_{aspan}}{CVR_m(CPP_m)/CVR_{min}} + C_{offset}$$

where.

C_{aspan} is a coefficient reflecting the sensitivity of C_a in response to changes in pressure,

C_{offset} is a constant allowing vertical translation of the C_a-CVR curve, and.

CVR_{min} is the minimum value of cerebrovascular resistance, during complete vasodilation at the lower limit of autoregulation.

Cv

The compliance of the venous compartment is modelled as a constant, as there is no data suggesting its non-linear character.

Rb

The resistance of venous outflow through the bridging veins is dependent on the pressure gradient P_v-P_i. Due to the small transmural pressure in the venous compartment, the bridging veins are modelled to be collapsible. The model of 'compression cost' (Piechnik, 2000) is chosen; it simulates the increase in vascular resistance due to a decrease in vascular lumen. This approach is adopted instead of the Starling resistor (Schoser et al., 1999) model, as the latter generated abnormally high ICP pulsatility (Piechnik, 2000). The resistance is expressed as the following:

$$R_b = \begin{cases} \frac{R_{b0}}{P_v - P_i} \; for \; P_v > P_i \\ 10000 \; for \; P_v < P_i \end{cases}$$

where.

R_{b0} is a scaling coefficient, and.

'10000' is an arbitrary constant term, simulating infinite resistance due to a complete blockage of venous outflow, when ICP exceeds the venous pressure.

CSF circulation

The CSF space is characterised by the intracranial compliance (C_i), rate of CSF formation (I_f), and resistance to CSF outflow (R_{CSF}). Both R_{CSF} and I_f are considered constants, while C_i is related to ICP and the elasticity of CSF space:

$$C_i = \begin{cases} \dfrac{1}{E(P_i - P_0)} & for\ P_i > P_{breakpoint} \\ \dfrac{1}{E\left(P_{breakpoint} - P_0\right)} & for\ P_i < P_{breakpoint} \end{cases}$$

where.

E is the elasticity of the CSF space,

$P_{breakpoint}$ is the pressure breakpoint between linear and non-linear range of cerebrospinal compliance, and.

P_0 is the pressure corresponding to infinite compliance, which essentially provides an offset to the inverse relationship between compliance and pressure.

C_i can also be defined as the change in intracranial volume with respect to ICP change. In other words, it is the derivative of the function V(P); its inverse function is commonly plotted as the pressure-volume curve (Fig. 8).

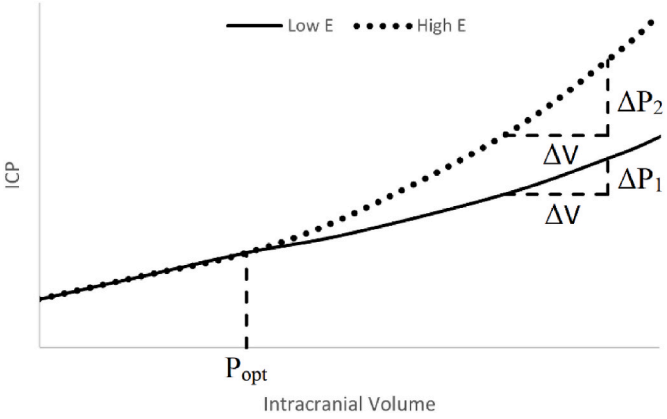

Fig. 8. The pressure-volume relationship of the CSF space, with C_i equals the reciprocal of its slope. Above the pressure linearity breakpoint (P_{opt}), CSF space with high elasticity has a lower value of C_i than that with low elasticity ($\Delta V/\Delta P_2 < \Delta V/\Delta P_1$).

The variations of CVR, C_a and C_i are plotted in Fig. 9 (Piechnik, 2000; Czosnyka et al., 1997) below.

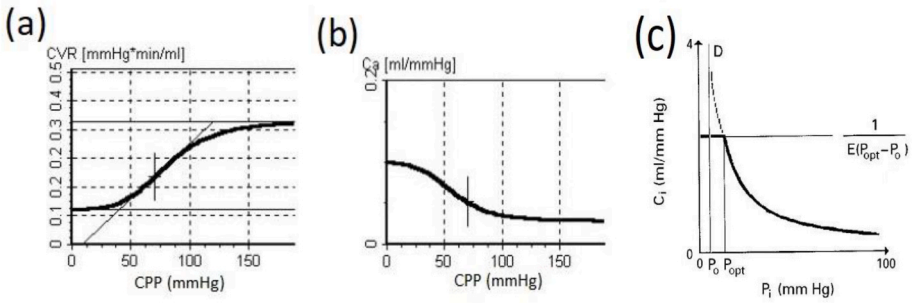

Fig. 9. Relationships of CVR (a) and C_a (b) with CPP, and C_i with P_i (c).

The table below summarises the values of the model parameters.

Table I
Values of parameters used for model simulations.

Model Parameter	Value
R_a (mmHg*min/mL)	0.1
CVR_{max} (mmHg*min/mL)	0.5
CVR_{min} (mmHg*min/mL)	0.1
CPP_{max} (mmHg)	95
CPP_{min} (mmHg)	55
CPP_{offset} (mmHg)	−30
C_{aspan} (mL/mmHg)	0.01
C_{offset} (mL/mmHg)	0.05
C_v (mL/mmHg)	1
R_{b0} (mmHg*min/mL)	0.5
E (1/mL)	0.05
P_0 (mmHg)	5
$P_{breakpoint}$ (mmHg)	10
I_f (mL/min)	0.3

Establishing Mathematical Relationships with the Electrical Analogue

The current (flow rate) and voltage (pressure) at different points of the circuit are of interest; they can be described mathematically with 'state equations'. These equations are derived from the electric model with the laws of electric circuits. In the implementation of this model, the Kirchhoff's principle of charge conservation was employed: the algebraic sum of all currents entering a junction is zero.

From the original model, three state equations can be established by considering the current at three nodes of the circuit (Fig. 1(b)):

At node A,

$$\frac{dP_a}{dt}=\frac{dP_i}{dt}+\frac{1}{C_a}\left(\frac{ABP-P_a}{R_a}-\frac{P_a-P_v}{CVR}-I_f\right)$$

At node B,

$$\frac{dP_v}{dt}=\frac{dP_i}{dt}+\frac{1}{C_v}\left(\frac{P_a-P_v}{CVR}-\frac{P_v-P_{ss}}{R_b}\right)$$

And at node C

$$\frac{dP_i}{dt}=\frac{1}{C_i}\left(\frac{ABP-P_a}{R_a}-\frac{P_v-P_{ss}}{R_b}-\frac{P_i-P_{ss}}{R_{CSF}}\right)$$

where P_a, P_v, and P_i are the cerebral arterial pressure, pial venous pressure, and intracranial pressure respectively.

There are no analytic solutions to this set of first-order differential equations, due to the non-linear dependence of some of its parameters (CVR, C_a, C_i, R_b) on the node pressures. Instead, the solutions were approximated by numerical integration, using the 4th order Runge-Kutta method (RK 4). RK 4 is an effective and accurate method for solving initial-value problems of differential equations. For an initial value problem

$$\frac{dy}{dt}=f(t,y),y(t_0)=y_0$$

the solution at the next step (y_{n+1}) is evaluated with the recursion formulae (Zheng and Zhang, 2017; Romeo, 2020)

$$y_{n+1}=y_n+\frac{h}{6}(k_1+2k_2+2k_3+k_4)$$

$$t_{n+1}=t_n+h$$

where

$$k_1=f(t_n,y_n)$$

$$k_2=f\left(t_n+\frac{h}{2},y_n+\frac{h}{2}k_1\right)$$

$$k_3=f\left(t_n+\frac{h}{2},y_n+\frac{h}{2}k_2\right)$$

$$k_4=f(t_n+h,y_n+hk_3)$$

where h is the step size (the time interval between two simulated data points); it was set as 40 ms in this study.

After substituting the relationships of the parameters into the three state equations and implementing the RK 4 method, the node pressures P_a, P_v and P_i can be evaluated. Also, the cerebral blood flow (CBF) through the middle cerebral artery can be calculated using the Ohm's law:

$$CBF=\frac{ABP-P_a}{R_a}$$

With the incorporation of the ISF compartment, the state equation at node C of the new model was modified:

$$\frac{dP_i}{dt}=\frac{1}{C_i}\left(\frac{ABP-P_a}{R_a}-\frac{P_v-P_{ss}}{R_b}-\frac{P_i-P_{ss}}{R_{CSF}}-\frac{P_i}{R_{ISF}}\right)$$

The state equations at nodes A and B remain the same.

References

Aaslid, R., Lindegaard, K.F., Sorteberg, W., Nornes, H., 1989. Cerebral autoregulation dynamics in humans. Stroke 20 (1), 45–52. https://doi.org/10.1161/01.STR.20.1.45.

Abbott, N.J., 2004. Evidence for bulk flow of brain interstitial fluid: significance for physiology and pathology. Neurochem. Int. 45 (4), 545–552. https://doi.org/10.1016/j.neuint.2003.11.006.

Boon, A.J.W., et al., 1997. Dutch normal-pressure hydrocephalus study: prediction of outcome after shunting by resistance to outflow of cerebrospinal fluid. J. Neurosurg. 87 (5), 687–693. https://doi.org/10.3171/JNS.1997.87.5.0687.

Børgesen, S.E., Gjerris, F., 1982. The predictive value of conductance to outflow of CSF in normal pressure hydrocephalus. Brain 105 (Pt 1), 65–86. https://doi.org/10.1093/BRAIN/105.1.65.

Brady, K.M., et al., 2012. Positive end-expiratory pressure oscillation facilitates brain vascular reactivity monitoring. J. Appl. Physiol. 113 (9), 1362–1368. https://doi.org/10.1152/japplphysiol.00853.2012.
Caire, F., Moreau, J.J., 2010. Méthode et résultats du test de perfusion dans l'hydrocéphalie à pression normale : revue de la littérature. Rev. Neurol. (Paris). 166 (5), 494–501. https://doi.org/10.1016/J.NEUROL.2009.10.007.
Claassen, J.A.H.R., Thijssen, D.H.J., Panerai, R.B., Faraci, F.M., 2021. Regulation of cerebral blood flowin humans: physiology and clinical implications of autoregulation. Physiol. Rev. 101 (4), 1487–1559. https://doi.org/10.1152/physrev.00022.2020.
Czosnyka, M., Piechnik, S., Richards, H.K., Kirkpatrick, P., Smielewski, P., Pickard, J.D., 1997. Contribution of mathematical modelling to the interpretation of bedside tests of cerebrovascular autoregulation. J. Neurol. Neurosurg. Psychiatry 63 (6), 721–731. https://doi.org/10.1136/jnnp.63.6.721.
Czosnyka, M., et al., 1999. Hemodynamic characterization of intracranial pressure plateau waves in head-injury patients. J. Neurosurg. 91 (1), 11–19. https://doi.org/10.3171/JNS.1999.91.1.0011.
Czosnyka, M., Czosnyka, Z., Momjian, S., Pickard, J.D., 2004. Cerebrospinal fluid dynamics. Physiol. Meas. 25 (5) https://doi.org/10.1088/0967-3334/25/5/R01.
Czosnyka, Z., Czosnyka, M., Lavinio, A., Keong, N., Pickard, J.D., 2008. Clinical testing of CSF circulation. Eur. J. Anaesthesiol. 25 (Suppl. 42), 142–145. https://doi.org/10.1017/S0265021507003249.
Daley, M.L., Leffler, C.W., Czosnyka, M., Pickard, J.D., 2005. Plateau waves: changes of cerebrovascular pressure transmission. Acta Neurochir. Suppl. (95), 327–332. https://doi.org/10.1007/3-211-32318-X_67.
Davson, H., Hollingsworth, G., Segal, M.B., 1970. The mechanism of drainage of the cerebrospinal fluid. Brain 93 (4), 665–678. https://doi.org/10.1093/BRAIN/93.4.665.
Doron, O., Zadka, Y., Barnea, O., Rosenthal, G., 2021. Interactions of brain, blood, and CSF: a novel mathematical model of cerebral edema. Fluids Barriers CNS 18 (1), 1–14. https://doi.org/10.1186/s12987-021-00274-z.
Drzewiecki, G., et al., 1997. Modeling in physiology Vessel growth and collapsible pressure-area relationship. Am. J. Physiol. Heart Circ. Physiol. 273, H2030–H2043.
Eklund, A., et al., 2007. Assessment of cerebrospinal fluid outflow resistance. Med. Biol. Eng. Comput. 45 (8), 719–735. https://doi.org/10.1007/s11517-007-0199-5.
Ekstedt, J., 1977. CSF hydrodynamic studies in man. 1. Method of constant pressure CSF infusion. J. Neurol. Neurosurg. Psychiatry 40 (2), 105. https://doi.org/10.1136/JNNP.40.2.105.
Hansen, A.J., Olsen, C.E., 1980. Brain extracellular space during spreading depression and ischemia. Acta Physiol. Scand. 108 (4), 355–365. https://doi.org/10.1111/j.1748-1716.1980.tb06544.x.
Hoffmann, O., 1987. Biomathematics of intracranial CSF and haemodynamics. Simulation and analysis with the aid of a mathematical model. Acta Neurochir. Suppl. (Wien) 40, 117–130. https://doi.org/10.1007/978-3-7091-8941-2_6/COVER.
Hrabětová, S., Hrabe, J., Nicholson, C., 2003. Dead-space microdomains hinder extracellular diffusion in rat neocortex during ischemia. J. Neurosci. 23 (23), 8351–8359. https://doi.org/10.1523/jneurosci.23-23-08351.2003.
Iliff, J.J., et al., 2014. Impairment of glymphatic pathway function promotes tau pathology after traumatic brain injury. J. Neurosci. 34 (49), 16180–16193. https://doi.org/10.1523/JNEUROSCI.3020-14.2014.
Kellie, G., 1824. An Account of the Appearances Observed in the Dissection of Two of Three Individuals Presumed to Have Perished in the Storm of the 3d, and Whose Bodies Were Discovered in the Vicinity of Leith on the Morning of the 4th, November 1821; with Some Reflection, vol. 1. Trans. Medico-Chirurgical Soc. Edinburgh, pp. 84–122.
Lalou, A.D., et al., 2020. Shunt infusion studies: impact on patient outcome, including health economics. Acta Neurochir. (Wien) 162 (5), 1019–1031. https://doi.org/10.1007/s00701-020-04212-0.
Liu, X., et al., 2020. Assessment of cerebral autoregulation indices – a modelling perspective. Sci. Rep. 10 (1), 1–11. https://doi.org/10.1038/s41598-020-66346-6.
Lundberg, N., 1962. Continuous recording and control of ventricular fluid pressure in neurosurgical practice. J. Neuropathol. Exp. Neurol. 21 (3), 489. https://doi.org/10.1097/00005072-196207000-00018, 489.
Mahajan, R.P., Simpson, E.J., 1998. Reliability of the Transient Hyperemic Response Test in Detecting Changes in Cerebral Autoregulation Induced by the Graded Variations in End-Tidal Carbon Dioxide. Neurosurg. Anesth.
Marmarou, A., Shulman, K., LaMorgese, J., 1975. Compartmental analysis of compliance and outflow resistance of the cerebrospinal fluid system. J. Neurosurg. 43 (5), 523–534. https://doi.org/10.3171/JNS.1975.43.5.0523.
Marmarou, A., Shulman, K., Rosende, R.M., 1978. A nonlinear analysis of the cerebrospinal fluid system and intracranial pressure dynamics. J. Neurosurg. 48 (3), 332–344. https://doi.org/10.3171/JNS.1978.48.3.0332.
Monro, A., 1783. Observations on the structure and functions of the nervous system. london Med. J. 4 (2), 113–135.
Oertel, J., Antes, S., 2013. Infusion studies in hydrocephalus. Acta Neurol. Scand. 127 (5), 360–361. https://doi.org/10.1111/ANE.12066.
Piechnik, S.K., 2000. A Mathematical and Biophysical Modelling of Cerebral Blood Flow and Cerebrospinal Fluid Dynamics, pp. 1–209 [Online]. Available: http://www.docudesk.com.
Ramirez de Noriega, F., et al., 2018. A swine model of intracellular cerebral edema - cerebral physiology and intracranial compliance. J. Clin. Neurosci. 58, 192–199. https://doi.org/10.1016/J.JOCN.2018.10.051.
Romeo, G., 2020. Mathematics for dynamic economic models. Elem. Numer. Math. Econ. with Excel 139–215. https://doi.org/10.1016/B978-0-12-817648-1.00004-9.
Rosner, M.J., Rosner, S.D., Johnson, A.H., 1995. Cerebral perfusion pressure: management protocol and clinical results. J. Neurosurg. 83 (6), 949–962. https://doi.org/10.3171/JNS.1995.83.6.0949.
Schoser, B.G.H., Riemenschneider, N., Hansen, H.C., 1999. The impact of raised intracranial pressure on cerebral venous hemodynamics: a prospective venous transcranial Doppler ultrasonography study. J. Neurosurg. 91 (5), 744–749. https://doi.org/10.3171/JNS.1999.91.5.0744.
Smielewski, P., Czosnyka, M., Iyer, V., Piechnik, S., Whitehouse, H., Pickard, J., 1995. Computerised transient hyperaemic response test-A method for the assessment of cerebral autoregulation. Ultrasound Med. Biol. 21 (5), 599–611. https://doi.org/10.1016/0301-5629(94)00154-6.
Syková, E., Nicholson, C., 2008. Diffusion in brain extracellular space. Physiol. Rev. 88 (4), 1277–1340. https://doi.org/10.1152/physrev.00027.2007.
Ursino, M., 1988a. A mathematical study of human intracranial hydrodynamics. Part 1–The cerebrospinal fluid pulse pressure. Ann. Biomed. Eng. 16 (4), 379–401. https://doi.org/10.1007/BF02364625.
Ursino, M., 1988b. A mathematical study of human intracranial hydrodynamics. Part 2–Simulation of clinical tests. Ann. Biomed. Eng. 16 (4), 403–416. https://doi.org/10.1007/BF02364626.
Ursino, M., Di Giammarco, P., 1991. A mathematical model of the relationship between cerebral blood volume and intracranial pressure changes: the generation of plateau waves. Ann. Biomed. Eng. 19 (1), 15–42. https://doi.org/10.1007/BF02368459.
Ursino, M., Lodi, C.A., 1997. A simple mathematical model of the interaction between intracranial pressure and cerebral hemodynamics. J. Appl. Physiol. 82 (4), 1256–1269. https://doi.org/10.1152/JAPPL.1997.82.4.1256.
Varsos, G.V., Kasprowicz, M., Smielewski, P., Czosnyka, M., 2014. Model-based indices describing cerebrovascular dynamics. Neurocrit. Care 20 (1), 142–157. https://doi.org/10.1007/s12028-013-9868-4.
Zheng, L., Zhang, X., 2017. Numerical methods. Model. Anal. Mod. Fluid Probl. 361–455. https://doi.org/10.1016/B978-0-12-811753-8.00008-6.